Small Phase Pattern 2D Beam Steering and A Single LCOS Design of 40 1×12 Stacked Wavelength Selective Switches

Haining Yang[1], Brian Robertson[1], Peter Wilkinson[1,2] and Daping Chu[1,2*]

[1]*Roadmap Systems Ltd, St John's Innovation Centre, Cowley Road, Cambridge, CB4 0WS, United Kingdom*
[2]*Photonics and Sensors Group, Department of Engineering, University of Cambridge, 9 JJ Thomson Avenue, Cambridge, CB3 0FA, United Kingdom*
[*]*daping.chu@roadmapsystems.co.uk*
[*]*dpc31@cam.ac.uk*

Abstract: Two-dimensional beam steering by small, square, phase patterns as small as 50×50 pixels on a phase-only liquid crystal on silicon (LCOS) device is experimentally verified as suitable for the application of wavelength selective switches (WSSs), in terms of the diffraction efficiency and steering accuracy. This enables a proposed highly functional and versatile stacked switch architecture, where 40 independent 1×12 WSSs can be realised on a single 4k LCOS device. They can be configured to support a 1×N WSSs with N≤144, or an N×N wavelength crossconnect with N≤12.

OCIS codes: (060.1810) Buffers, couplers, routers, switches, and multiplexers; (050.1970) Diffractive optics.

References and links

1. T. A. Strasser, and J. L. Wagener, "Wavelength-selective switches for ROADM applications," IEEE J. Sel. Top. Quantum Electron. **16**(5), 1150-1157 (2010).
2. D. M. Marom, D.T. Neilson, D.S. Greywall, P. Chien-Shing, N.R. Basavanhally, V.A. Aksyuk, D.O. Lopez, F. Pardo, M.E. Simon, Y. Low, P. Kolodner, and C.A. Bolle, "Wavelength-selective 1×K switches using free-space optics and MEMS micromirrors: theory, design, and implementation," J. Lightwave Technol. **23**(4), 1620-1630 (2005).
3. M. Sharma , P. Hansen , B. Nayer, and P. Wigley, "Next-generation ROADM technologies and architecture," Proc. SPIE **8283**, 828309 (2012).
4. B. C. Collings, "Advanced ROADM Technology and Architecture," in *Optical Fiber Communication Conference*, OSA Technical Digest (online) (Optical Society of America, 2015), paper Tu3D.3.
5. Z. Zhang, Z. You, and D. Chu, "Fundamentals of phase-only liquid crystal on silicon (LCOS) devices," Light-Sci. Appl. **3**, e213 (2014).
6. S. Frisken, G. Baxter, D. Abakoumov, H. Zhou, I. Clarke, and S. Poole, "Flexible and grid-less wavelength welective wwitch using LCOS technology," in *Optical Fiber Communication Conference/National Fiber Optic Engineers Conference*, OSA Technical Digest (CD) (Optical Society of America, 2011), paper OTuM3.
7. M. A. F. Roelens , S. Frisken , J. A. Bolger , D. Abakoumov , G. Baxter , S. Poole, and B. J. Eggleton, "Dispersion trimming in a reconfigurable wavelength selective switch," J. Lightwave Technol. **26**(1), 73-76 (2008).
8. B. Robertson, H. Yang, M. M. Redmond, N. Collings, J. R. Moore, J. Liu, A. M. Jeziorska-Chapman, M. Pivnenko, S. Lee, A. Wonfor, I. H. White, W. A. Crossland, and D. P. Chu, "Demonstration of multi-casting in a 1 × 9 LCOS wavelength welective switch," J. Lightwave Technol. **32**(3), 402-410 (2013).
9. S. Frisken , H. Zhou , D. Abakoumov , G. Baxter , S. Poole , H. Ereifej, and P. Hallemeier, "High performance 'drop and continue' functionality in a wavelength selective switch," in *Optical Fiber Communication Conference/National Fiber Optic Engineers Conference*, OSA Technical Digest (CD) (Optical Society of America, 2006), paper PDP14.
10. J. Schröder, M. A. F. Roelens, L. B. Du, A. J. Lowery, S. Frisken, and B. J. Eggleton, "An optical FPGA: reconfigurable simultaneous multi-output spectral pulse shaping for linear optical processing," Opt. Express **21**(1), 690–697 (2013).
11. M. Johansson, S. Hård, B. Robertson, I. Manolis, T. Wilkinson, and W. Crossland, "Adaptive beam steering implemented in a ferroelectric liquid-crystal spatial-light-modulator free-space, fiber-optic switch," Appl. Opt. **41**(23), 4904-4911 (2002).

12. H. Yang, B. Robertson, D. P. Chu, "A non-intrusive in situ method of optical beam profiling in LCOS-based optical fiber switches," Opt. Lasers Eng. **51**(7), 916-920 (2013).
13. Z. Zhang, H. Yang, B. Robertson, M. Redmond, M. Pivnenko, N. Collings, W. A. Crossland, and D. Chu, "Diffraction based phase compensation method for phase-only liquid crystal on silicon devices in operation," Appl. Opt. **51**(17), 3837-3846 (2012).
14. B. Robertson, Z. Zhang, M. M. Redmond, N. Collings, J. Liu, R. Lin, A. M. Jeziorska-Chapman, J. R. Moore, W. A. Crossland, and D. P. Chu, "Use of wavefront encoding in optical interconnects and fiber switches for cross talk mitigation," Appl. Opt. **51**(5), 659-668 (2012).
15. B. Robertson, Z. Zhang, H. Yang, M. M. Redmond, N. Collings, J. Liu, R. Lin, A. M. Jeziorska-Chapman, J. R. Moore, W. A. Crossland, and D. P. Chu, "Reduction of crosstalk in a colourless multicasting LCOS-based wavelength selective switch by the application of wavefront encoding," Proc. SPIE **8284**, 82840S (2012).
16. B. Robertson, Z. Zhang, H. Yang, M. M. Redmond, N. Collings, J. Liu, R. Lin, A. M. Jeziorska-Chapman, J. R. Moore, W. A. Crossland, and D. P. Chu, "Application of the fractional Fourier transform to the design of LCOS based optical interconnects and fiber switches," Appl. Opt. **51**(12), 2212-2222 (2012).
17. B. Robertson, H. Yang, M. M. Redmond, N. Collings, J. Liu, A. M. Jerziorska-Chapman, J. R. Moore, Z. Zhang, W. A. Crossland, A. Wonfor, I. H. White, S. H. Lee, and D. Chu, "The Use of Wavefront Encoding to Reduce Crosstalk in a Multicasting Fiber Telecom Switch," *Optical Fiber Communication Conference*, OSA Technical Digest (CD) (Optical Society of America, 2012), paper OM2J.6.
18. H. Yang, B. Robertson, and D. Chu, "Crosstalk reduction in holographic wavelength selective switches based on phase-only LCOS devices," *Optical Fiber Communication Conference*, OSA Technical Digest (CD) (Optical Society of America, 2014), paper Th2A.23.
19. H. Yang, B. Robertson, and D. Chu, "Transient Crosstalk in LCOS Based WSS and a Method to Suppress the Crosstalk Levels," in *Optical Fiber Communication Conference/National Fiber Optic Engineers Conference*, OSA Technical Digest (CD) (Optical Society of America, 2013), paper OW1C.3.
20. H. Yang, B. Robertson, D. Yu, Z. Zhang, and D. P. Chu, "Origin of Transient Crosstalk and Its Reduction in Phase-only LCOS Wavelength Selective Switches," J. Lightwave Technol. **31**(23), 3822-3829 (2013).
21. C. Pulikkaseril , L. A. Stewart , M. A. F. Roelens , G. W. Baxter , S. Poole, and S. Frisken, "Spectral modeling of channel band shapes in wavelength selective switches," Opt. Express **19**(9), 8458-8469 (2011).
22. K. Suzuki, Y. Ikuma, E. Hashimoto, K. Yamaguchi, M. Itoh, and T. Takahashi, "Ultra-High Port Count Wavelength Selective Switch Employing Waveguide-Based I/O Frontend," in *Optical Fiber Communication Conference*, OSA Technical Digest (online) (Optical Society of America, 2015), paper Tu3A.7.
23. Y. Ikuma, K. Suzuki, N. Nemoto, E. Hashimoto, O. Moriwaki, and T. Takahashi, "8 × 24 Wavelength Selective Switch for Low-loss Transponder Aggregator," in *Optical Fiber Communication Conference Post Deadline Papers*, OSA Technical Digest (online) (Optical Society of America, 2015), paper Th5A.4.
24. M. Iwama, M. Takahashi, Y. Uchida, M. Kimura, R. Kawahara, S. I. Matsushita, and T. Mukaihara, "Low loss 1×93 wavelength selective switch using PLC-based spot size converter," in *Proceedings of European Conference on Optical Communication (ECOC)* (IEEE, 2015), pp. 1–3.
25. L. Zong, H. Zhao, Z. Feng, and Y. Yan, "8×8 Flexible Wavelength Cross-Connect for CDC ROADM Application," IEEE Photonics Technol. Lett. 27(24), 2603-2606, (2015).
26. J. Tsai, S. Huang, D. Hah, and M. C. Wu, "Wavelength-selective $1\times N^2$ switches with two-dimensional input/output fiber arrays," in *Conference on Lasers and Electro-Optics/Quantum Electronics and Laser Science Conference*, Technical Digest (Optical Society of America, 2003), paper CTuQ4.
27. J. Tsai and M. C. Wu, "$1\times N^2$ wavelength-selective switches with high fill-factor two-axis analog micromirror arrays," in *Optical Fiber Communication Conference*, Technical Digest (CD) (Optical Society of America, 2004), paper MF42.
28. J. Tsai, S. Huang, D. Hah and M. C. Wu, "$1\times N^2$ wavelength-selective switch with telescope-magnified 2D input/output fiber collimator array," in *Conference on Optical MEMS, 2003 IEEE/LEOS International*, 2003, pp. 45-46.
29. Y. Ishii, K. Hadama, J. Yamaguchi, Y. Kawajiri, E. Hashimoto, T. Matsuura, and F. Shimokawa, "MEMS-based 1×43 wavelength-selective switch with flat passband," in *35th European Conference on Optical Communication*, Vienna, 2009, pp. 1-2.
30. M. P. Dames, J. R. Collington, W. A. Crossland, and R. W. A. Scarr, "The design and interconnection of a free-space photonic/electronic ATM switching module," in *Proceedings of IEEE/LEOS Summer Topical Meetings on Advanced Applications of Lasers in Materials Processing/Broadband Optical Networks/Smart Pixels/Optical MEMs and Their Applications* (IEEE, 1996), pp. 101-102.
31. T. Nguyen, J. An, J. Choi, and N. Kim, "A Hybrid Algorithm to Reduce the Computation Time of Genetic Algorithm for Designing Binary Phase Holograms," J. Opt. Soc. Korea **7**(4), 264-268 (2003).
32. D. Sinefeld and D. M. Marom, "Insertion Loss and Crosstalk Analysis of a Fiber Switch Based on a Pixelized Phase Modulator," J. Lightwave Technol. **29**, 69-77 (2011).
33. J. Goodman, *Introduction to Fourier Optics* (Roberts & Company Publishers, 2005).
34. K. L. Tan, W. A. Crossland, and R. J. Mears, "Dynamic holography for optical interconnections. I. Noise floor of low-cross-talk holographic switches," J. Opt. Soc. Am. A **18**(1), 195-204 (2001).

35. K. L. Tan, S. T. Warr, I. G. Manolis, T. D. Wilkinson, M. M. Redmond, W. A. Crossland, R. J. Mears, and B. Robertson, "Dynamic holography for optical interconnections. II. Routing holograms with predictable location and intensity of each diffraction order," J. Opt. Soc. Am. A **18**(1), 205-215 (2001).
36. Thorlabs F240APC-1550, http://www.thorlabs.de/thorproduct.cfm?partnumber=F240APC-1550.
37. Jasper Display JD2552, http://www.jasperdisplay.com/products/detail/245/
38. Jasper Display JD2704, http://www.jasperdisplay.com/products/detail/377/
39. ITU G.694.1 : Spectral grids for WDM applications: DWDM frequency grid, https://www.itu.int/rec/T-REC-G.694.1-201202-I/en
40. H. Yang, B. Robertson, P. Wilkinson, and D. Chu, "Stacked Wavelength Selective Switch Design for Low-cost CDC ROADMs," to be presented in *Optoelectronics and Communications Conference / International Conference on Photonics in Switching*, (Optical Society of America, 2016), paper ME2.
41. M. Furuya, R. Sterling, W. Bleha and Y. Inoue, "D-ILA® Full Resolution 8K Projector," *SMPTE Tech Conference & Expo, 2009 Annual*, Hollywood, CA, USA, 2009, pp. 1-9.

1. Introduction

A wavelength selective switch (WSS) [1,2] is one of the key enabling technologies for reconfigurable optical networks [3,4]. A typical WSS is able to selectively route individual wavelength division multiplexing (WDM) channels entering its input fibre port to any of the output fibre ports according to the software configuration that is remotely controlled by the service providers. In recent years, phase-only liquid crystal on silicon (LCOS) spatial light modulators (SLMs) [5] have become the technology of choice for WSSs, due to its software upgradable nature and support for flexible spectrum switching [6], dispersion compensation [7], multicasting [8-10], and adaptive alignment [11-13]. Various efforts have been made to improve both the optical performance and the switching functionalities of the LCOS WSSs, especially in terms of static [14-18] and transient [19-20] crosstalk reduction, passband shape optimisation [21] and port count increase [22-25].

WSSs are usually based on the 'disperse-and-select' optical design, where the WDM channels from the input port are diffracted by a static grating along the dispersion axis at the plane of the optical engine, i.e. LCOS device, before being subsequently switched to the target output ports according to the sub-holograms, i.e. diffractive phase patterns, displayed on the corresponding areas of the LCOS device. Due to the limited number of pixels available on the current generation LCOS devices, however, anamorphic optics are invariably used in these designs to convert the beams of individual WDM channels into elongated shape at the LCOS plane. Correspondingly, output ports are arranged along the switching axis, which is orthogonal to the dispersion axis. Although such an approach is able to increase the port count in one axis, it fails to fully exploit the two dimensional (2D) nature of the pixel array on the LCOS device. Moreover, for such a configuration, all the undesirable diffraction orders due to the LCOS defects will also appear along this switching axis, which makes it fundamentally difficult to suppress crosstalk, especially in WSSs with high port counts. It should also be pointed out 2D output port arrangement and beam steering has been previously demonstrated in WSSs based on 2-axis analogue micro mirror array technologies [26-29]. However, WSSs based on micro mirror array technologies became less attractive in recent years due to its incompatibility with the flexible spectrum switching that is required by next generation networks.

In this paper, we demonstrate the 2D beam steering capability of the small sub-hologram with a square shape in a proof-of-concept LCOS WSS setup without using anamorphic optics. We further propose a stacked WSS design with 2D output port arrangement, which enables a single 4k LCOS device to realise up to 40 independent 1×12 WSSs within one module. Applications of this WSS module are also discussed.

2. 2D beam steering

2.1 Principle of 2D beam steering

The conventional Fourier transform optical system shown in Fig. 1 is used to illustrate the beam steering principle of the LCOS device. In this system, the IN/OUT plane and the LCOS

device are placed at the front and back focal planes of the collimating lens (L_1), respectively. The Gaussian beam waist at the LCOS plane, i.e. ω_{SLM}, can be expressed by

$$\omega_{SLM} = f_1\lambda/(\pi\omega_{IN/OUT}). \quad (1)$$

where $\omega_{IN/OUT}$ is the input Gaussian beam waist at the IN/OUT plane; f_1 the focal length of L_1; and λ the wavelength.

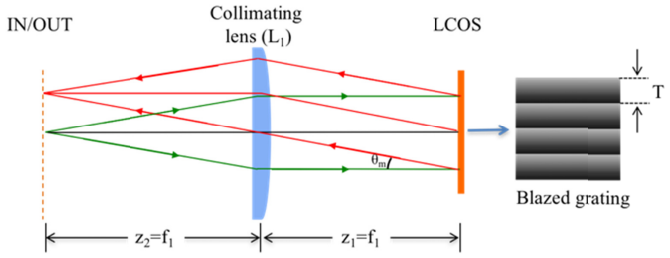

Fig. 1. Beam steering by an LCOS device in the conventional Fourier transform optical system.

The LCOS device displays a phase hologram to steer input beam into an offset position at the IN/OUT plane. The dimension ($x_H \times y_H$) of this hologram should ideally be greater than $3\omega_{SLM}$ so that at least 99% of the input power is contained within the sub-hologram. Although various algorithms [30,31] exist to generate such holograms, blazed gratings are most commonly used in case of single-direction beam steering. Similar to Eq. (1), the relationship between the offset position (δ_O) at IN/OUT plane and the period (T) of the blazed grating can be expressed as

$$\delta o = f_1\lambda/T. \quad (2)$$

The hologram should also cover at least three periods of grating, i.e. x_H>3T and y_H>3T, so that the input and output beams at the IN/OUT plane can be sufficiently separated. In addition, the blazed grating displayed on the LCOS device is quantised due to its pixelated nature and therefore the actual diffraction efficiency of such a grating is also dependent on the number of pixels within one period. An extensive study on the effect of pixilation and phase quantisation on the beam steering performance of the LCOS device had been carried out previously [32]. Although the performance of the LCOS based optical switches also depends on the optical design, in general, a minimum period of 7 pixels is required to maintain a reasonably high efficiency (>90%) [33] and low crosstalk. Taking all these factors in account, the minimum dimension of hologram required for beam steering in an optical switch equals to 21 pixels, which leads to 2 switchable positions along one axis.

In the WSS employing LCOS devices with HD definition, i.e. 1920×1080 pixels, only 24 pixels along the dispersion axis can be allocated to each 50 GHz channel so that the whole C-band with 80 such channels can be covered. In order to achieve required passband shape, the beam size of the signal along the dispersion axis needs to be smaller than 24 pixels. As a result, it is impossible to steer the signal along the dispersion. By introducing anamorphic optics, the signal beam can be significantly elongated along the axis that is orthogonal to the dispersion axis while its size is maintained along the dispersion axis. Consequently, the number of switchable positions is increased along this orthogonal axis, i.e. the switching axis.

With the availability of LCOS devices with 4k definition, however, 50 pixels can be allocated to each 50 GHz channel so that the signal beam can be steered along arbitrary axis. Therefore, at least 8 possible output port positions can be uniformly arranged on a 2D Cartesian grid by employing a modulo 2π algorithm [34,35] to generate blazed grating with non-integral period values. Figure 2 compares the blazed gratings with periods of 10.00 pixels

and 10.01 pixels under the assumption that the LCOS device in use has 240 unique phase levels between 0 and 2π. Due to its pixelated nature, the LCOS device performs a spatial quantisation on the blazed gratings and the resulted phase pattern will apparently have the same period of 10 pixels as shown in Fig.2. However, the phase values for certain pixels are different. By analysing their associated replay fields, it can be concluded that even such small difference in the phase profile leads to ~5 μrad angular deviation in the diffraction order and <0.01 dB change in the diffraction efficiency. Experimental verification of this calculation is described out in the following sections.

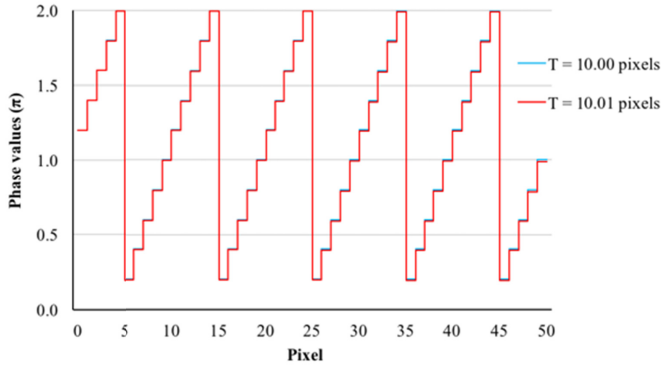

Fig. 2. Phase patterns of blazed gratings with periods of 10.00 and 10.01 pixels.

The relationship between switchable positions and the unique phase levels available on the LCOS device is also studied numerically. In the ideal case of continuous phase change, there can be unlimited number of grating periods between 9 and 11 pixels in theory. The quantisation of phase levels will limit the actual number of sub-holograms that can be displayed in practice, hence there will be a finite number of switching positions in the system. First of all, 200,000 theoretical phase profiles were generated in the form of blazed gratings with periods between 9 and 11 pixels. The phase quantisation of various degrees was applied to these phase profiles before their corresponding replay fields were calculated using the Fourier transform. By analysing the positions of the +1st diffraction orders of quantised phase profiles, the number of switchable positions can be obtained. The results were shown in Fig. 3. It can be seen that the number of switchable positions available increases almost linearly as the phase level increases at a rate of about 15 additional switchable positions per extra phase

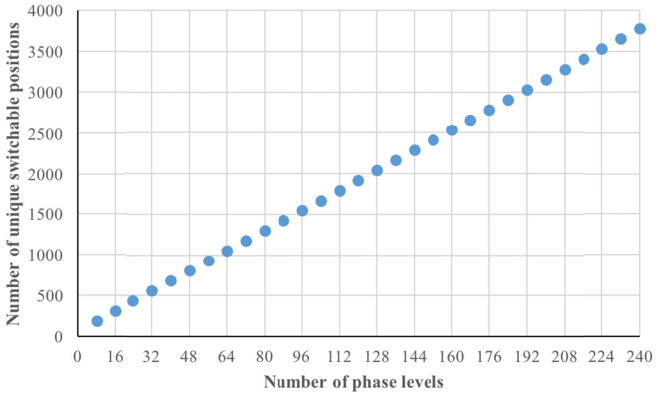

Fig. 3. The relationship between the number of unique switchable positions and the number of phase levels available on the LCOS device.

level for a 50×50 sub-hologram. This apparent linearity can be associated with the linear increase of the number of possible sub-holograms as the number of phase levels increases. With 240 phase levels, more than 3700 switchable positions can be achieved as the grating period increases from 9 to 11 pixels. This is more than enough for the WSS application and can be further utilised for active alignment to reduce alignment errors and manufacturing costs.

2.2 Experimental setup

A proof-of-concept optical system with wavelength selective switching capability is built to verify the 2D beam steering performance of holograms with such a dimension. As shown in Fig. 4, the signal beams enter this system via a single-mode SMF28 fibre. the lens L_1 in this system convert the input Gaussian beam waist of ω_f at the fibre facet to a Gaussian beam waist of ω_G at the transmissive DEMUX grating plane. This static grating serves as the dispersive element that angularly separates the wavelengths channels. Subsequently, the lens L_2 transforms this angular separation into the positional offset between the wavelength channels at the LCOS plane, i.e. the beams of wavelength channels will illuminate separate areas on the LCOS device, where holograms with corresponding dimensions will be displayed. The holograms for each individual wavelength channel will be referred to as sub-holograms throughout the rest of this paper. In this specific experiment, the separation between two adjacent 50 GHz channels is 50 pixels on the LCOS with a pixel size of 6.4 μm along the dispersion axis, which is also referred to as horizontal axis. In the absence of anamorphic optics, the dimension of each sub-hologram in the vertical axis is 50 pixels as well. By ensuring the DEMUX grating and the LCOS device are placed at the front and back focal planes of L_2, respectively, the beams of all the wavelength channels will be normally incident on the LCOS SLM with a Gaussian beam waist of ω_{SLM}. The signal beams will be diffracted by their corresponding sub-holograms through an angle and propagate back to the DEMUX grating at a position offset from the incident beam. A two-lens imaging system (L_3 and L_4) is used to create an image of the field at the DEMUX grating at the test plane. Such setup offers great flexibility for the evaluation of the beam steering performance of square sub-holograms. At the test plane, we can view the replay field with a camera to observe a shift in the position of the beam and the appearance of other diffraction orders. Alternatively, we can also use fibre-coupled power meter to assess diffraction efficiency and crosstalk levels.

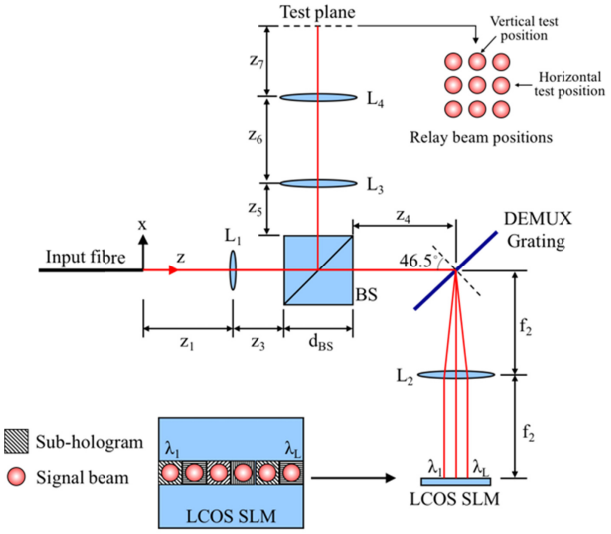

Fig. 4. Optical setup for evaluating 2D beam steering by small sub-holograms on LCOS devices.

2.3 Beam steering performance

In the analysis on the beam steering performance, we assume the sub-holograms are in the form of standard blazed gratings, which steer the signal beam in either horizontal axis or vertical axis. 201 unique test sub-holograms, whose grating periods increase from 9 pixels to 11 pixels in a step of 0.01 pixels, are generated for the vertical axis switching and horizontal axis switching, respectively.

Firstly, an adjustable aperture on a translation stage is put at the test plane, which only allows the $+1^{st}$ diffraction order to pass through. A power meter is placed immediately after the aperture to measure the diffraction efficiency of the test sub-holograms. The results show that the diffraction efficiency will gradually decrease from 87% to 80% as the grating period changes from 11 pixels to 9 pixels. The trend is consistent with the theory [33]. More importantly, the diffraction efficiencies only varies <0.2 dB when the beam was steered along different directions, e.g. vertical, horizontal or 45-degree, etc. The crosstalk from the -1^{st} diffraction order of these blazed gratings was measured to be <-20 dB. Further improvement on the crosstalk suppression is required. However, it should also be pointed out that these crosstalk levels were measured using a free-space power meter in this test system. In the actual fibre switches, the fibre coupling effect would further reduce the crosstalk levels. Moreover, reflection and scattering from the large number of optical surfaces in this test system would also raise the background crosstalk levels.

In the second test, a near-field camera for infrared wavelengths is placed at the test plane to capture the replay field. By employing 2D Gaussian fitting on the beams of the $+1^{st}$ diffraction order of the test sub-holograms, the central positions of these beams can be accurately identified and compared. It is assumed that the target output position in either axis at the test plane corresponds to the $+1^{st}$ diffraction order position of the blazed grating with a period of 10 pixels. Figure 5 shows relationship between the grating periods in the test sub-holograms and the corresponding $+1^{st}$ diffraction order's offset from the target position in the horizontal axis and vertical axis, respectively. In either direction, a grating period of 9 pixels will cause the beam to shift away 0.45 mm with respect to the target position while a grating period of 11 pixels will lead to 0.33 mm deviation. Again this is consistent with the theoretical relationship described by Eq. (2). As mentioned in the previous section that the difference between the sub-holograms used in this work that have adjacent period values is very small. However, it is evident from Fig. 5 that such small difference does consistently lead to positional offset at the replay field in the actual optical system.

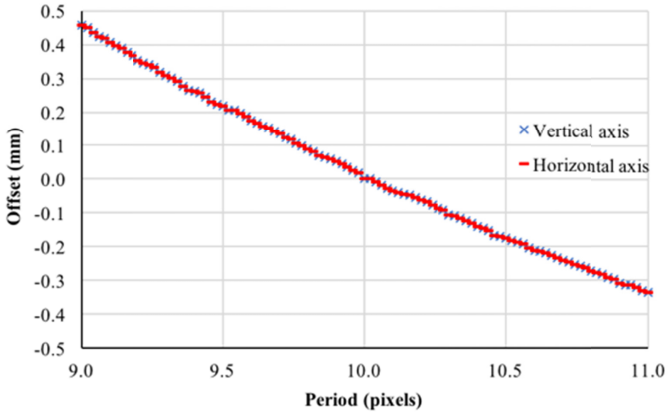

Fig. 5. The relationship between the grating period and $+1^{st}$ diffraction order beam's offset from the target position in both horizontal and vertical directions.

The experimental beam steering positions shown in Fig. 5 is compared with theoretical positions calculated by Eq. (2) and the results are shown in Fig. 6. It can be seen that the discrepancy between the experimental and theoretical values are less than 5 μm in the majority of cases. This can be primarily attributed to the error introduced in the camera operation. The infrared camera used in this experimental work was a 1.3Mpixel CMOS sensor that had a phosphor coating to enhance sensitivity in the C-band. The camera had a pixel size of 5.2 μm and the phosphor layer coated on its CMOS sensor would increase the effective pixel size, however, the beam centre of the beam was found though a 2D Gaussian fitting algorithm applied to the +1st diffraction order beam (size of ~192 μm). This is to identify the beam centre more accurately but it introduces errors when the beam is not Gaussian.

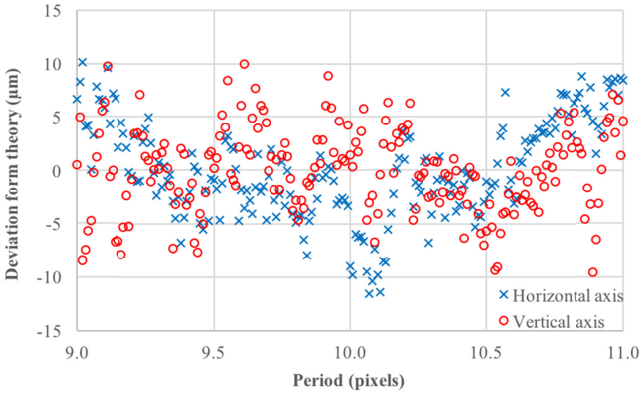

Fig. 6. The experimental deviation from the theoretical beam steering position.

In a further test, a fibre collimator [36] is placed a position at test plane where the +1st diffraction order of the sub-hologram with a grating period of 10 pixels can achieve optimal coupling into the fibre. The optical power that is coupled into the fibre is measured by a fibre-coupled power meter as the LCOS SLM is cycled through all 201 test sub-holograms described above. This process is repeated for both axes as well and the normalised results are plotted in Fig. 7, which shows consistency between them. The asymmetry in the roll-off of the coupled power is due to the grating period deviating from the target 10 pixels and is a reflection of the asymmetric offset in the +1st diffraction order position shown in Fig. 5.

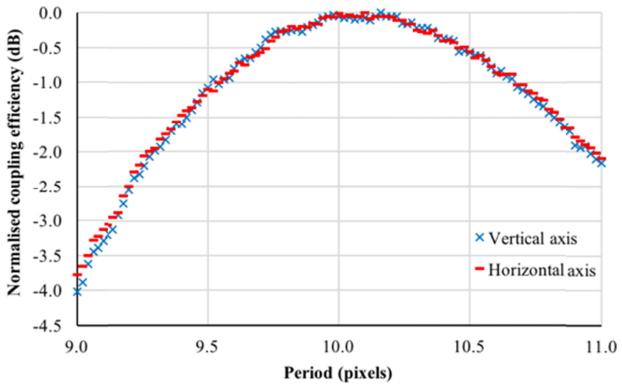

Fig. 7. The relationship between the grating period in both horizontal and vertical directions and the optical power coupled into the corresponding fibres.

In conclusion, the results obtained in these three tests confirm that the small square sub-holograms are able to accurately steer the signal beam in a WSS in two dimensions with equally high performance. It is worth mentioning that the performance achieved in this section is based on an LCOS device assembled at the Photonics and Sensors Group, University of Cambridge, using a Jasper 2k backplane [37]. The key parameters that determine the performance of the LCOS device includes pixel size, liquid crystal material, cell thickness and uniformity and the anti-reflective coating coverplate glass, etc. While these parameters are kept same, the pixel count itself doesn't affect the beam steering performance. Therefore, there is no reason to believe a 4k LCOS device would perform differently on this regard. Since a 4k LCOS device with the same key specifications is currently under development for the switching system described in the next section, this 2k LCOS device is suitable for evaluating the 2D beam steering performance of small square holograms in a wavelength selective switching system.

3. Stacked WSS design

Without using anamorphic optics, the number of pixels required along the vertical axis of the LCOS SLM is significantly reduced. In order to fully exploit the pixel count along this axis, a stacked WSS design is hence proposed.

3.1 Design Principle

The principle of the design is shown in Fig. 8(a), 8(b) and 8(c), which depicts M stacked 1×N WSSs with an array of objective lenses (L_A), a relay system (L_1 and L_2) and DEMUX optics (P_g), with M=3 and N=8 in this example, respectively. Each of the M stacked 1×N WSSs has a fibre array cluster, which consists of 1 input, N output fibre ports and the corresponding micro-lens array. These clusters are arranged along the y-axis, each acting as an independent 1×N WSS, with each input light beam illuminating a spatially distinct row of sub-holograms (e.g., S_1, S_2, and S_3). The WDM input is launched into each WSS via the central fibre in the corresponding cluster. The objective lens generates a beam waist of radius ω_o at plane P_o. The 4f relay system images this beam waist at the SLM plane (P_{SLM}). The static grating (P_g) imparts an angular displacement of $\beta_G(\lambda)$ to each wavelength channel in the x-z plane. Signal beams associated with these wavelengths illuminate separate sub-holograms displayed on the LCOS device. The sub-hologram for a wavelength channel could be a grating of period T, orientated at an angle of φ with respect to the local xy-coordinate system, that diffracts the light beam such that it leaves the LCOS SLM with a propagation vector of k(ρ, φ, λ), where ρ is the angle of the vector with respect to the local z-axis. The diffracted beam is

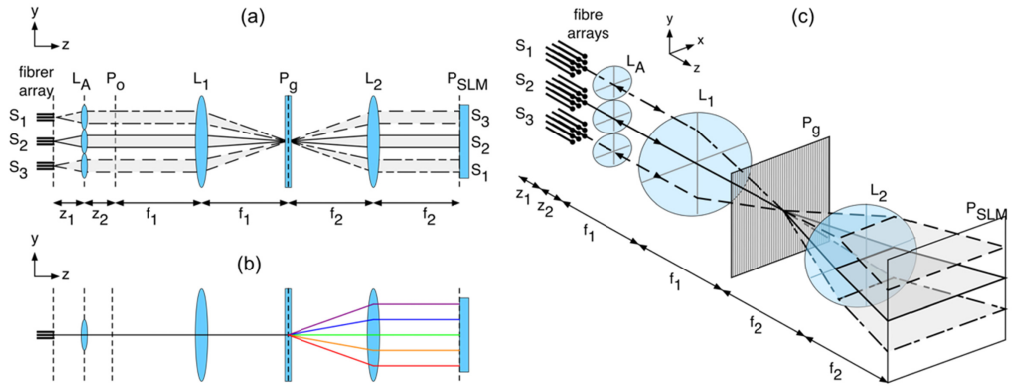

Fig. 8. Design principle for the stacked WSSs based on a single LCOS device, (a) side view, (b) top view, and (c) system view.

subsequently imaged at P_o by the relay system. The objective lens in the output optics shown in Fig. 9 converts the propagation vector of a wavelength channel, k(ρ, φ, λ), to a beam position that is offset from the optical axis. The angle is controlled such that the beam is concentric with respect to the intended output fibre, thereby maximising coupling efficiency as shown in Fig. 9(a). The high beam steering accuracy by small square sub-hologram demonstrated in the previous part of this paper is critical for this part of operation. A secondary lenslet array, L_F, focuses the wavelength channels into the output fibre array.

As mentioned, by using a standard 4k LCOS device, we can allocate 50×50 pixels for each 50 GHz channel within the C-band, which means that at least 40 (48 in the case of Jasper JD2704 with 4096x2400 pixels [38]) independent WSSs can be stacked on a single LCOS device along the y-axis. If multiple LCOS devices are tiled along the y-axis, the number of independent WSSs that can be stacked based on this design principle can be further increased. The minimum channel bandwidth increment is 1 GHz per pixel, which complies with ITU G.694.1 standard [39] for bandwidth variable wavelength selective switching. In the absence of anamorphic optics, the un-modulated input signal to each sub-hologram has a circular beam shape on P_{SLM}, which is designed to cover 31×31 pixels and achieve the 4^{th} order super Gaussian passband shape. The small number of pixels covered by the beam limits the maximum grating period to 10 pixels, which is larger than the minimum period of 7 pixels required to realise sufficient switching efficiency and reasonably low crosstalk level for two switchable positions along a given direction. The circular beam on P_{SLM} allows 2D steering, giving 8 switchable output ports arranged on a Cartesian grid, as shown in Fig. 9(b). The number of the switchable output ports can be further increased, given the same beam steering range, to 12 if the fibre ports are arranged in a hexagonal pattern as shown in Fig. 9(c).

It is should be noted that the input ports of these stacked WSSs is off the optical axis of the whole system. As a result, the input beams will enter the static grating (P_g) with different angles. Due to the conical diffraction, the spectra of the input WDM signals from the stacked WSSs will be slightly bended to various degrees on the LCOS plane, i.e. the beam of each WDM channels from a same WSS will have different positions along the y-axis on the LCOS plane. This may potentially reduce maximum number of WSSs that can be stacked in this design. In our design, however, the offset with respective to the optical axis, i.e. 14 mm in maximum, is very small compared with optical path, i.e. 300 mm, required to disperse the WDM signals adequately on the LCOS plane. As a result, such a difference in the beam positions within a WSS is maintained less than 3 pixels in the worst-case scenario. Considering 50 pixels along the y-axis is allocated to each stacked WSS and the only 31 pixels of them are used to cover at least 99% power of each beam, our design has sufficient number of pixels to cope with this effect. Therefore, conical diffraction will not leave any impact on the number of the WSSs that can be stacked in this design.

3.2 Optical performance

Crosstalk from an LCOS blazed grating occurs due to quantization of the phase pattern and by pixel fringing fields, where the electric field due to the voltage applied to a pixel leaks across to neighbouring pixels. The edge effect in the LCOS device can lead to a series of discrete diffraction orders of a blazed grating, which may coincide with a number of fibre

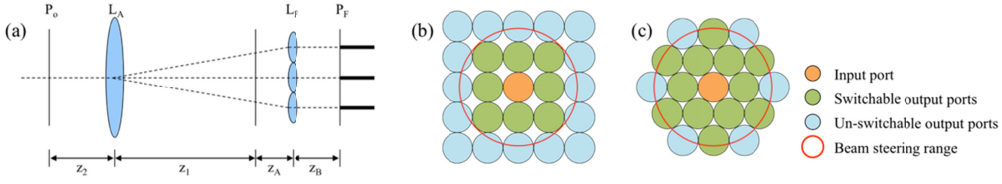

Fig. 9. (a) Output optics design; 2D beam steering over the fibre ports arranged on (b) a Cartesian grid and (c) a hexagonal grid.

ports in the conventional LCOS WSS design employing a one-dimensional linear fibre port array and anamorphic optics, leading to crosstalk. In the design illustrated in Fig. 8, however, only the - 1st diffraction order of the blazed grating can coincide with an un-targeted port in either the quadratic or hexagonal arrangement. In this specific case, the -1st diffraction order will give arise a crosstalk of about -20 dB, which can be suppressed by using advanced computer generated hologram algorithms for a specific order [18]. In addition, the incorporation of the wavefront encoding technique has been demonstrated to be able to suppress crosstalk effectively by introducing an optical asymmetry into the system [14,15,17]. It should also be noted that the individual WSSs in this design do not share the same output lenslet element, L_A, which is responsible for coupling the beam into the target fibre efficiently only if the beam wavefront at P_o matches a pre-designed requirement. Therefore, it is extremely difficult for the beams from the adjacent WSSs to introduce extra crosstalk.

One of the advantages of the design illustrated in Fig. 8 is the ability to individually steer each wavelength channel in two-dimensions. As a result, we can compensate for system misalignment errors on a per-channel basis by actively optimising the propagation vector of each beam, $k(\rho,\varphi,\lambda)$. The insertion loss of the switch extrapolated from LCOS SLM measurement data and current commercial component data is summarised in Table 1.

Table 1. 1×N WSS switch power budget

Component	Transmission	Passes	Loss (dB)
System components (Fresnel losses)	0.93	2	-0.63
DEMUX grating	0.90	2	-0.92
Intrinsic LCOS reflectivity	0.85	1	-0.70
LCOS and axicon diffraction efficiency	0.65	1	-1.87
System alignment	0.90	1	-0.46
Total			**-4.58**

In order to address the concerns regarding the passband shapes when switching the signal beam in 2D, the passbands were analysed for this stacked WSS design. Figure 10 shows the passband shapes for a 50 GHz channel at the wavelength of 1550.12 nm when it is being switched along the dispersion axis and along a direction orthogonal to the dispersion axis, respectively. It can be seen that these two passbands are almost identical to each other, which can lead to the conclusion that the beam steering direction in the WSS based on 'disperse-and-switch' optical architecture doesn't affect the passband. In addition, these simulation results also predict that our stacked WSS design is able to achieve -0.5 dB passband of 36 GHz and -3.0 dB passband of 46 GHz.

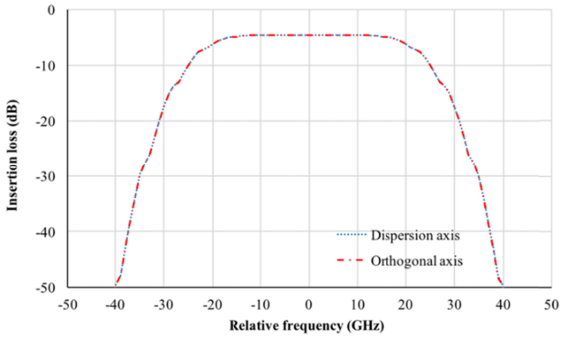

Fig. 10. Passband shapes when the signal is switched to a port in the direction (a) along the dispersion axis and (b) orthogonal to dispersion axis, respectively.

To investigate whether intrinsic passband ripples will occur due to the limited number of grating periods covered, a detailed simulation of the wavelength response of a sub-hologram was performed while switching along both the dispersion and orthogonal axis. The results are shown in Fig. 11. It can be seen that switching along the dispersion axis will not introduce additional passband distortion when compared to switching along the orthogonal axis. It should be stressed that the unmodulated beams of central wavelengths within a signal channel will covers at least three periods of the beam steering blazed grating in this design. As a result, it is impossible that a given wavelength only covers the flyback region of the blazed grating, which would cause intrinsic passband ripples in addition to any other system distortions.

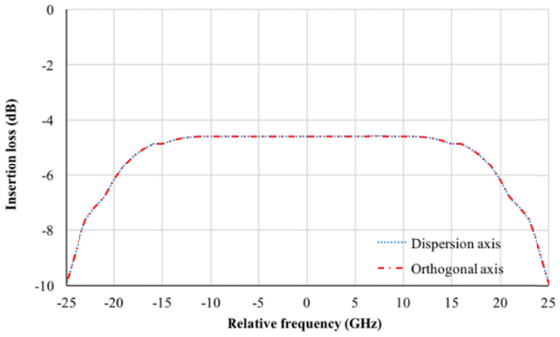

Fig. 11. Detailed passband tops when the signal is switched to a port in the direction (a) along the dispersion axis and (b) orthogonal to dispersion axis.

It should be noted that the performance analysis in this section is based on the LCOS device we evaluated in Section 2 of this paper, which has a pixel size of 6.4 μm. Although the design principle we described can be applied on LCOS device with any specifications, however, the optical performance of the stacked WSSs will inevitably depend on the performance of the LCOS device itself. By using LCOS devices with smaller pixel sizes, the total optical path can be reduced, which will lead to a smaller footprint of the whole system. However, the fringing field effect is stronger in the LCOS devices with smaller pixel sizes. This will impact the insertion loss and crosstalk levels. To reduce the fringing field effect, liquid crystal materials with higher birefringence index could be used in this case.

3.3 Potential applications

The large number of independent WSSs as designed in this module allows various potential applications. The WSSs can be used independently in a conventional reconfigurable optical add/drop multiplexer (ROADM) architecture, greatly reducing size and cost. By cascading the WSSs as shown in Fig. 12(a), the module becomes a WSS with a significantly higher port count. For example, 13 of the 40 1×12 WSSs within this module can construct a 1×144 WSS. In total, the module can deliver 3 such WSSs. Although the insertion loss in this configuration will be doubled, it would be comparable to the level reported in those WSSs with such a large port count [22], while offering fundamentally lower cross talk by the two-pass spatial filtering.

It is also possible to build a wavelength cross-connect (WXC) by connecting the output ports between several WSSs. Fig. 12(b) gives an example of 4×4 WXC, in which each WSS still has 8 spare ports for adding or dropping wavelengths to or from corresponding directions. Our module is able to realise 12×12 WXC using 24 of the independent WSSs. Such a switching module is able to realise non-blocking WSSs between multiple input and output ports with high efficiency, which is key to achieve colourless-directionless-contentionless (CDC) ROADMs [40].

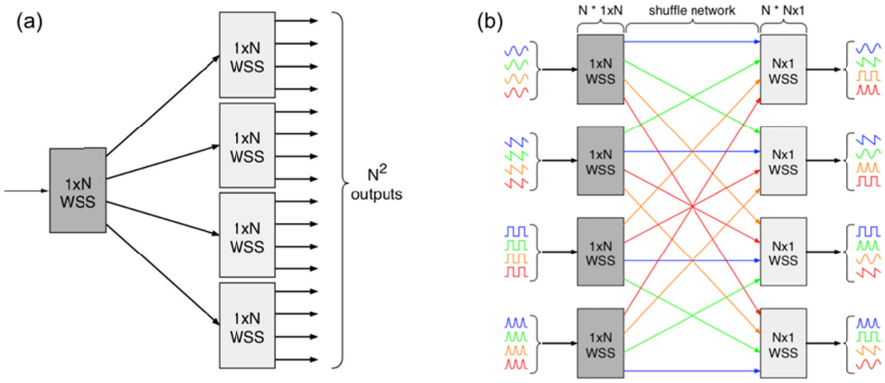

Fig. 12. (a) The cascaded configuration for high port count WSS; (b) 4×4 WXC with extra 8 add/drop ports for each direction.

4. Discussion and Conclusion

We have presented experimental results to show accurate and efficient 2D beam steering can be achieved by using square sub-holograms as small as 50×50 pixels on a phase-only LCOS device. The effect of the phase levels available on the number of switchable positions is analysed to show the linear relationship between them. In a proof-of-concept testing system using an LCOS device with 240 phase levels, >80% diffraction efficiency and 5 μrad angular resolution has been demonstrated for all the 200 unique sub-holograms used in the test, where the periods vary between 9 and 11 pixels in either vertical and horizontal axes.

Based on these results, a stacked WSS architecture is proposed, in which 40 independent 1×12 WSSs can be realised in a single 4k LCOS device. The insertion loss of each 1×12 WSS is estimated to be -4.58 dB due to the ability of accurate 2D beam steering. The crosstalk in such WSS is primarily due to -1st diffraction order of the sub-holograms, which can be further reduced by using advanced hologram generation algorithms and wavefront encoding techniques plus novel optical design. The passband by using such a small sub-hologram is expected to comply with the ITU G.694.1 standard, with a channel bandwidth increment of 1 GHz or better. This architecture is highly flexible and can be reconfigured as cascaded 1×N WSSs with N up to 144, or an N×N WXC with N up to 12, or any combination thereof.

By integrating a large number of independent WSSs in a single LCOS device based on 2D beam steering, the proposed architecture can maximise the switching capability in terms of port count per pixel and minimise the cost and energy consumption per port. It also provides a flexible and versatile platform for bandwidth-variable formats in future ITU grid.

It should be noted that 2D beam steering with a square sub-hologram smaller than 50×50 pixels is possible. In fact, 21×21 pixels can be used to steer the beam to 4 positions. The reason for choosing 50×50 pixels in this work is because 50 is the maximum number of pixels along the wavelength axis that can be allocated to each 50 GHz channel in a 4k LCOS based WSS without anamorphic optics, which can give a maximum port count of 12 while maintaining a good beam steering accuracy and passband shape.

The stacked WSSs design presented in this paper can also be easily modified to cover a larger spectrum, i.e. C-band + L-band, to accommodate the needs of future telecommunication networks. By using the emerging 8k LCOS device [41], the spectrum coverage can be doubled. It is also possible to introduce anamorphic optics to slightly elongate the beams along the axis orthogonal to the dispersive axis so that the LCOS device would have enough pixels along the dispersive axis to cover the additional spectrum, although there would be trade-off between the spectrum coverage, port count within each WSS and number of WSSs that can be stacked. However, the number of WSSs that can be stacked could be increased by tiling multiple LCOS devices along the orthogonal axis.